Surface Science 602 (2008) 3588–3594

Contents lists available at ScienceDirect

Surface Science

journal homepage: www.elsevier.com/locate/susc

Sign-inverted surface stress-charge response in nanoporous gold

Hai-Jun Jin [a,*], Smrutiranjan Parida [a], Dominik Kramer [a], Jörg Weissmüller [a,b]

[a] Forschungszentrum Karlsruhe, Institut für Nanotechnologie, P.O. Box 3640, 76021 Karlsruhe, Germany
[b] Universität des Saarlandes, Technische Physik, Saarbrücken, Germany

ARTICLE INFO

Article history:
Received 13 August 2008
Accepted for publication 25 September 2008
Available online 8 October 2008

Keywords:
Gold
Porous solids
Nanostructures
Surface stress
Solid-liquid interfaces
Electrochemical phenomena

ABSTRACT

The surface stress-charge coefficient, ς, quantifies the response of the surface stress – a fundamental property of solid surfaces – to the addition or removal of superficial electric charge. So far, all experiments have found ς negative at clean metal surfaces. Here we report in situ dilatometry experiments on nanoporous gold samples prepared by dealloying. The results reveal a large reversible elastic contraction during the anodic part of cyclic potential scans. The behavior, which indicates an abnormal positive sign of ς, can be linked to a monolayer of strongly adsorbed oxygen formed during dealloying, and to the extraordinarily small (1–2 nm) structure scale of the material while the oxide is in place. After cathodic reduction, ς reverts to the conventional, negative sign of the clean metal surface. We discuss the sign of ς in relation to the electronic screening at metallic and oxide-covered surfaces.

1. Introduction

The surface stress, f, measures the forces by which the surface of a solid interacts elastically with the underlying bulk crystal lattice. Its magnitude is of current interest since f is intricately related to the surface electronic structure and bonding, and since it is relevant for reconstruction as well as for the stress in thin film devices [1–3]. At electrode surfaces, f varies as a function of the potential, E, or of the superficial charge density, q. Significant surface-induced stresses in the bulk are required for balancing the change in the surface forces, and the resulting strain is large enough to suggest the application of nanoporous metals as electrochemical actuators [4–6]. Current research in electrochemistry investigates the distinction between the potential- or charge dependence of f and of the surface tension, of which f is the strain derivative [7]. Contrary to the quadratic variation of $\gamma(q)$, practically all recent experiments find a linear $f(q)$ at metal surfaces near their potential of zero charge [3–5,8,9]. The surface stress-charge coefficient, $\varsigma = \mathrm{d}f/\mathrm{d}q|_e$ with e a tangential strain variable, is invariably found negative. In other words, for all that is known from experiment, metal surfaces tend to expand laterally when charged positively. This trend is confirmed by density functional theory (DFT) computation [10,11]. Yet, no arguments have emerged so far from these studies that would require ς to be negative under all circumstances. In fact, porous carbons as well as carbon nanotubes exhibit a parabolic variation of the strain with charge [12–14]. The difference underlines the importance of the nature of the bonding in the solid surface for the coupling between surface stress and excess charge. Here, we explore the charge response of the reversible strain during potential cycling for nanoporous gold (npg) samples prepared by dealloying [15]. We find that freshly prepared samples contract when charged positively, indicating an unusual, positive value of ς. The behavior can be related to an oxide layer which is formed during corrosion, and after reduction the surface recovers the conventional, negative-valued ς. In a companion study [16], similar findings are reported for granular nanoporous Pt, where a superficial oxide film can be grown by anodic cycling.

2. Experimental procedures

The master alloy $Ag_{75}Au_{25}$ (at.%) was arc melted from high purity Au and Ag wires (Au 99.9985% and Ag 99.99%, Chempur) and then homogenized at 950 °C for 50 h (sealed in quartz tube). Rectangular samples about $1.8 \times 1 \times 1$ mm^3 in size were cut from the ingot and annealed at 850 °C for 1.5 h under Ar for recovery. Nanoporous gold samples were prepared by dealloying this material in freshly prepared 1 M $HClO_4$ (using deionized ultra-pure water with electrical resistively of 18.2 MΩ cm^2/cm) and under potentiostatic control (PGSTAT 100, EcoChemie) at 850 mV versus a Ag/AgCl reference electrode. The Ag/AgCl electrode used in this study is a pseudo-reference electrode, whose potential with respect to standard Ag/AgCl electrode (3 M KCl solution) is 240 mV and 220 mV in 1 M $HClO_4$ and 0.3 M NaF, respectively. To minimize silver contamination in the sample compartment, the coiled-Ag wire counter electrode (CE) was separated from the main cell by placing it in a tube filled with the same solution and mounted with its opening close to the sample, as shown in Fig. 1b. The dealloying was

* Corresponding author.
E-mail address: haijun.jin@int.fzk.de (H.-J. Jin).

0039-6028/$ - see front matter © 2008 Elsevier B.V. All rights reserved.
doi:10.1016/j.susc.2008.09.038

stopped when the current fell to 10 μA. To this end the tube with the CE was removed, along with the electrolyte, while holding the sample at the dealloying potential. The cell was repeatedly rinsed with fresh 1 M $HClO_4$ to remove traces of Ag ions in solution, and strain measurements were performed in 1 M $HClO_4$ using different potential intervals as explained below.

Both the dealloying and the subsequent in situ measurement of strain during cyclic voltammetry were performed with an electrochemical cell of 10 ml volume in the sample space of a dilatometer (Linseis). Fig. 1 shows the schematic illustration and the picture of the electrochemical cell arranged in the dilatometer [17]. The sample remained in place in the dilatometer during the entire procedure. The dilatometer contact force was 20 cN and temperature was controlled to 18 °C.

X-ray diffraction was performed in Bragg–Brentano geometry using Cu Kα radiation and a position-sensitive detector. The scan covered the Au(1 1 1) and (2 0 0) Bragg reflections. $Ag_{75}Au_{25}$ was used as the master alloy for all diffraction measurements, see details in Ref. [18].

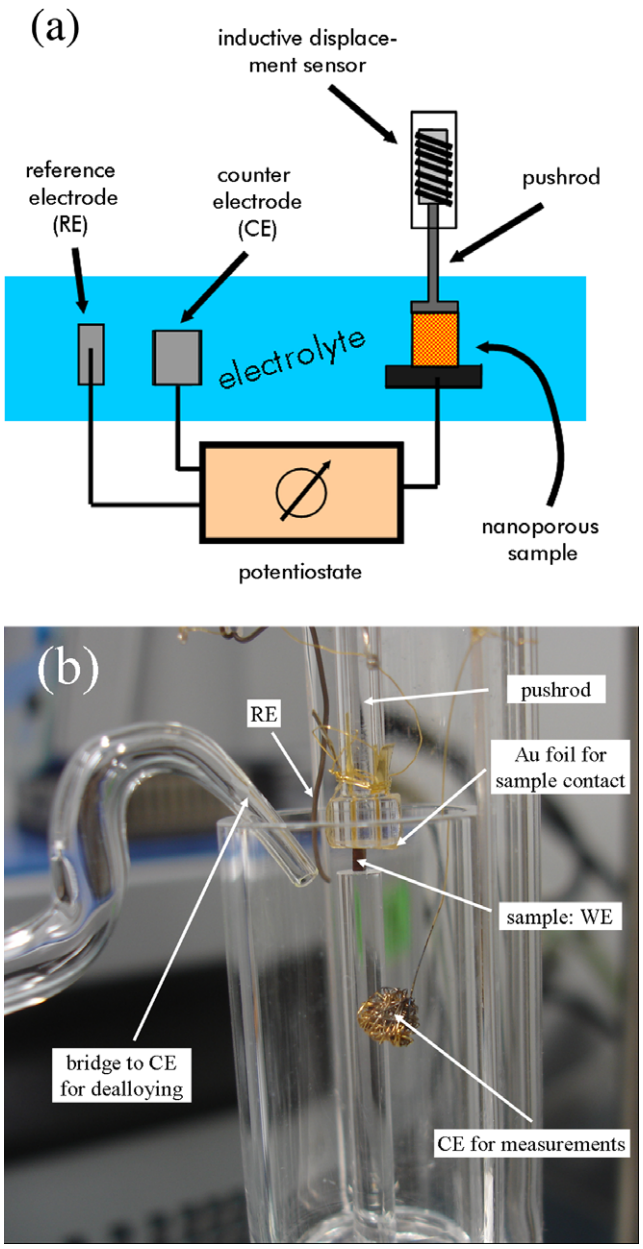

Fig. 1. The (vertical) dilatometer equipped with an electrochemical cell used in this study. (a) A schematic illustration of dilatometery measurement carried out in situ in an electrochemical environment. (b) Picture of electrochemical cell used in dilatometer. A glass tube was filled with electrolyte acting as a bridge to an external silver coil (not shown) counter electrode, which was only used for dealloying in order to minimize the silver contamination. Another piece of clean nanoporous gold was then connected as counter electrode for further measurements (it was not connected during dealloying).

3. Results

In several exploratory studies, in situ dilatometry experiments conducted immediately after the synthesis by dealloying gave quite different potential-strain curves compared to those after repeated electrochemical cycling. To systematically study this phenomenon we performed a first set of experiments, carefully avoiding potentials significantly more negative than E_D. A series of cathodic scans was then performed, and a second series of in situ strain measurement was carried out for comparison.

3.1. Dilatometry in as-prepared state

Fig. 2 shows results of in situ dilatometry in 1 M $HClO_4$ immediately after dealloying. The potential interval was centered near E_D (scan range 0.70 V to 1 V). The voltammogram is featureless and well reproducible, consistent with a charging that is reversible (in the sense that charge is conserved, and Faradaic processes – which involve electron transfer across the interface – are insignificant) and with a state of the surface which is stable during the voltammograms. A well reproducible length change is observed, with expansion in the anodic sweep. In other words, the graphs of strain versus potential and charge exhibit negative slopes.

3.2. Voltammetry during cathodic sweep

Fig. 3a shows a series of fifteen successive potential cycles, extending down to 0 V at their cathodic end and executed subsequent to those of Fig. 2. The first scan started at E_D scanning initially anodic. Important anion desorption is evidenced by the large negative value of the current, I, in its cathodic branch. The negative I persists through a major part of the anodic part of the scan, indicating that the anion desorption is slow and irreversible. This signature remains apparent throughout the first seven scans, while the voltammogram gradually evolves towards a more reproducible behavior. In view of the known phenomenology of the oxidation of Au in aqueous electrolytes [19], and of previous reports of oxide formation during dealloying [20], the irreversible process documented here can be understood as the reduction of a superficial oxide layer.

The cumulative charge, Q_C, transferred at the end of each cycle is shown in Fig. 3b. It is seen that Q_C saturates after about six cycles, at a value of about 5.0 C. Anticipating our experimental results (see below) for the mass-specific surface area, α_M, we work with $\alpha_M = 150\ m^2/g$. Assuming two electrons per desorbed (O^{-2}) ion, defining one equivalent monolayer (ML) as the density of Au atoms on a Au(1 1 1) surface, 13.9 nm^{-2}, and accounting for the sample mass of 6.334 mg, we may estimate the number of equivalent monolayers of oxygen removed. The result, shown as the right ordinate in Fig. 3b, saturates at 1.2 ML of oxygen, well compatible with our notion of a superficial oxide layer in the as-prepared samples.

3.3. Evolution of surface area

Superimposed to the irreversible reduction, the scans in Fig. 3a indicate the cyclic adsorption/desorption of OH, consistent with

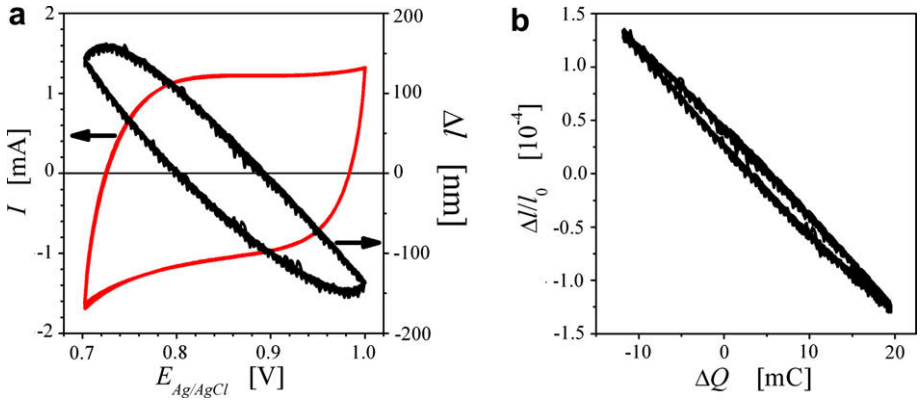

Fig. 2. Measurements in 1 M $HClO_4$ before cathodic potential sweep. (a) Current I versus potential E (left ordinate) and length change Δl (right ordinate) during cyclic voltammogram at 10 mV/s in potential range 0.7 V to 1 V. (b) Corresponding values of strain, $\Delta l/l_0$, versus net charge ΔQ. All parts show ten successive scans superimposed, indicating excellent reproducibility.

the established behavior of polycrystalline Au surfaces in $HClO_4$ [17,21]. It is seen that the area under the adsorption/desorption peaks decreases from scan to scan. This suggests that the number of adsorption sites decreases, as would be the case during coarsening of the porous microstructure. The largest decrease is apparent during the first scan, where the desorption feature in the cathodic leg of the scan is very much larger than in the subsequent ones. Apparently, the most important coarsening occurs practically instantaneously, during the first scan.

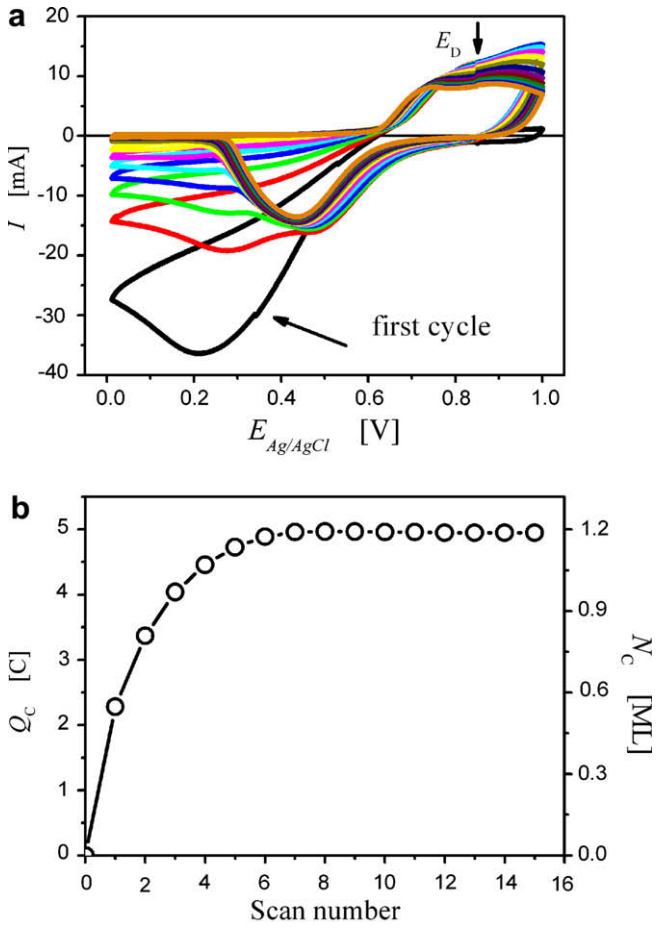

Fig. 3. Results of cathodic potential sweep in 1 M $HClO_4$. (a) Current I versus potential E during 15 successive cyclic at 10 mV/s. Negative Faraday current diminishes between successive cycles. (b) Cumulative charge-transferred, Q_C, at the end of each scan (left) and cumulative amount, N_C, of oxygen removed (right) after each cycle.

The evolution of the net surface area can be studied in more detail via the capacitance ratio method [22]. Here, α_M is determined by dividing the total differential capacity of the sample by the double-layer capacitance (capacity per area), c, of the planar gold surface. Impedance measurements [23] indicate values of 40 μFcm^{-2} and 20 μFcm^{-2}, respectively, for c at clean and oxide-covered Au surfaces. Narrow potential intervals (100 mV) within constant-current regions of the CV were chosen in order to minimize the contributions from charge-transfer reactions. The current values in the anodic and cathodic branches were found to be linear functions of the potential scan rate, indicating that the transport kinetics in the pore space do not affect the charging. The differential capacitance was determined by linear regression to graphs (Fig. 4b and d) of the sums of absolute currents versus scan rate. The values of α_M, before and after cathodic scanning are 150 (±5) m^2/g and 10 (±2) m^2/g, respectively. The latter is quite consistent with the AC impedance measurements in similar nanoporous gold samples [24]. Thus, the surface area is found reduced by a factor of ca. 15 after removing the superficial oxide layer.

The values of volume-specific surface area, α_V (per volume of the solid phase) corresponding to the above-mentioned α_M are 2.9 and 0.19 nm^{-1}. Nanoporous gold exhibits a bicontinuous microstructure, consisting of interpenetrating pore space and solid phase. The solid skeleton structure is formed by elongated 'ligaments' with roughly circular cross-section, connected in nodes [5,15]. An order of magnitude estimate of the characteristic structure size is obtained by considering idealized, cylindrical ligaments with diameter D and, hence, $\alpha_V = 4/D$. This yields $D = 1.4$ and 21 nm, respectively, before and after reduction. Whereas the final value is well consistent with findings from electron microscopy (see, for instance, [5,16]), the initial one is extraordinarily small. Apparently, such small ligaments sizes are only stable for the oxide-covered surface, and their observation may require in situ experiments during or immediately after dealloying.

3.4. Dilatometry after cathodic sweep

The in situ dilatometry measurement was repeated with 'clean' surfaces, subsequent to the removal of the superficial oxide layer by cathodic sweeping as described above. Two potential ranges were chosen: one (+0.7 V to +1.05 V) similar to that of Fig. 2, and a second (−0.3 V to +0.4 V) near the nominally capacitive charging region of the voltammogram.

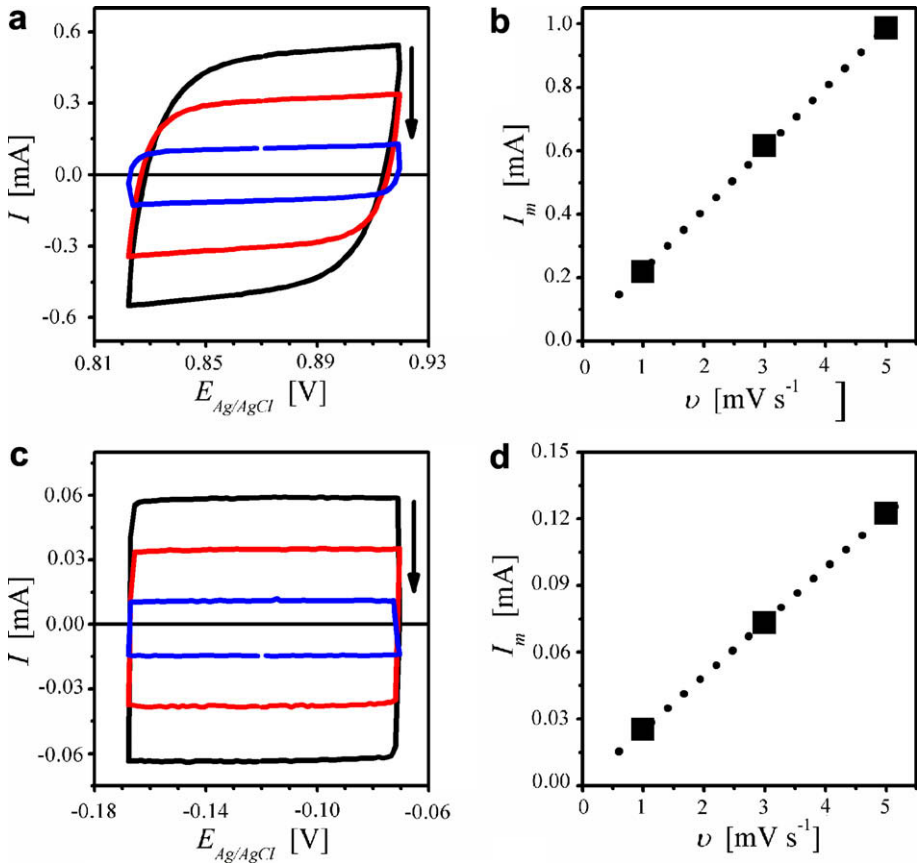

Fig. 4. Cyclic voltammograms in small potential ranges (ca.100 mV) at different scan rates (υ) in 1 M $HClO_4$, and current versus scan rate plots, before and after cathodic reduction. (a) CV at 5, 3 and 1 mV/s from +0.82 V to +0.92 V before cathodic sweep (ref. Fig. 2), (b) average of absolute current (I_m) at the middle of CVs in (a) versus scan rate, (c) CV at 5, 3 and 1 mV/s from −0.17 V to −0.07 V after cathodic sweep, (d) average of absolute current (I_m) at the middle of CVs in (c), at different scan rate. Arrows in (a) and (c) indicate direction of decreasing scan rates. Dotted lines in (b) and (d) are linear regression of respective I_m versus υ plots. Slope of I_m versus υ gives the capacitance in respective potential region. Capacitance before cathodic scan is about ten times larger than that after cathodic scan.

As shown in Fig. 5, the behavior is now qualitatively different. Firstly, for the more anodic potential interval – which can be compared to that of Fig. 2 – the amplitudes of charge as well as strain have decreased, by about the factors of 6 and 20, respectively. Secondly and most importantly, there is a qualitative change in the length-versus-charge graph: its slope changes sign, from contraction during anodic scans with the oxide-covered surface to expansion for the clean surface.

3.5. Experiments with NaF electrolyte

In a similar experiment, after dealloying in 1 M $HClO_4$ as above, strain measurements and cathodic scanning were carried out in 0.3 M aqueous solution of NaF, subsequent to careful washing to remove traces of $HClO_4$ and of Ag ions. The results (Fig. 6) agree qualitatively with those shown above: A negative strain-charge response was observed right after dealloying, as for as-prepared samples in $HClO_4$ but in a wider potential range. Here the strain amplitude (approximately 0.24%) and net charge were larger than those in $HClO_4$, by factors about 10 and 4, respectively. After cathodic scanning, the conventional, positive strain- charge response was recovered, as above. We have found that the lentil-shape of the voltammogram in Fig. 6a is characteristic of double-layer charging for nanoporous metals in solutions of low conductivity. This feature has been attributed to potential gradients in the electrolyte within the pore space, and to incomplete equilibration of the charge [25]. This implies that the 0.24% strain amplitude at 10 mV/s scan rate represent a lower bound of the strain that can be reached in this potential interval if the scan is slow enough to reach electrical equilibrium.

3.6. X-ray diffraction experiment

A diffraction experiment was carried out to check for the signature of a bulk gold oxide phase in dealloyed samples. The master alloy was here cut form a rolled and subsequently annealed sheet of Ag–Au, providing a larger sample size for the diffraction experiment. The bulk nanoporous gold sample was transferred to the diffractometer immediately after completion of dealloying at 850 mV (versus Ag/AgCl) in 1 M $HClO_4$. Fig. 7 shows the diffractograms of master alloy and nanoporous sample. The primary change in the diffractogram is a broadening of the Bragg reflections after dealloying. This broadening can be attributed to the formation of nano-ligaments, which essentially reduces the size of the coherently scattering regions of crystal lattice. The ratio of integrated reflection intensities in 111- and 200-peaks remains unchanged, indicating the retention of the strong 100-texture – a result of the rolling – in the master alloy.

The expected signature of a bulk oxide is the appearance of the most intense Au_2O_3 diffraction peak, at around 30° scattering angle [26]. No such feature was found. Furthermore, the data do not show a significant increase in the diffuse background, which would indicate an amorphous bulk oxide. Thus, the diffraction data do not support the existence of a separate oxide phase. They are, however, compatible with the existence of an epitaxial oxide layer at the surface.

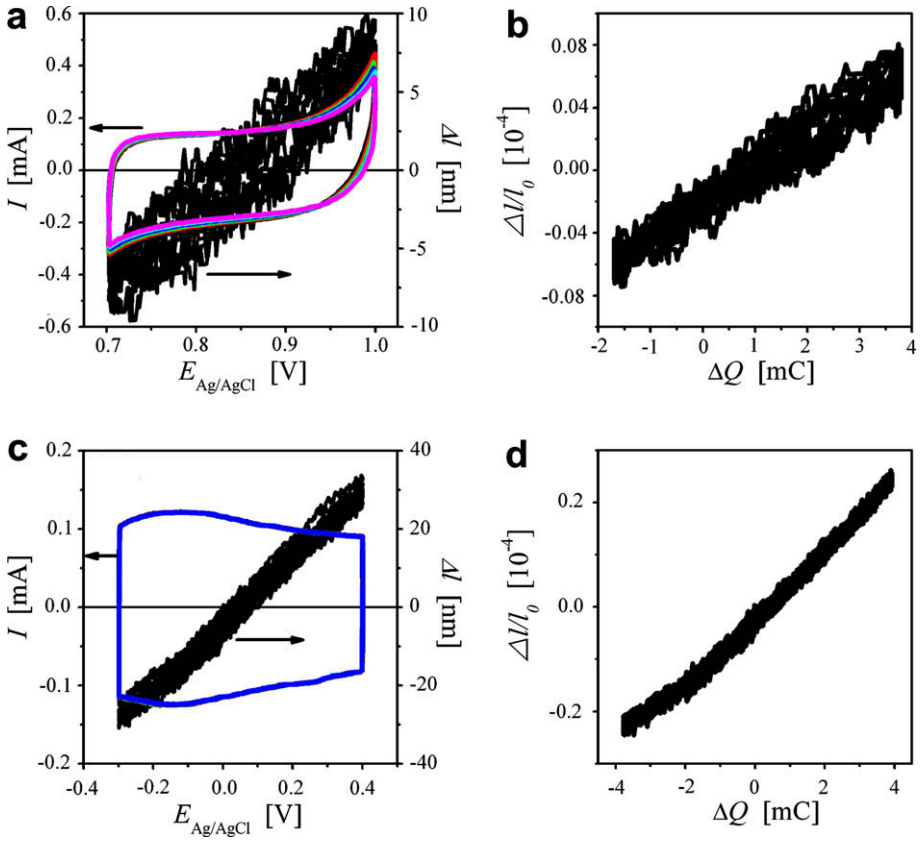

Fig. 5. Measurements in 1 M $HClO_4$ as in Fig. 1 but after cathodic potential sweep. (a) Cyclic voltammogram and length change with potential range 0.7 V to 1 V at 10 mV/s, (b) in situ strain, $\Delta l/l_0$, versus superficial surface charge derived from data in (a). (c) Cyclic voltammogram and length change in potential range −0.3 V to +0.4 V at 10 mV/s, (d) $\Delta l/l_0$ versus superficial surface charge derived from (c).

4. Discussion

The important observations of the previous section can be summarized as follows: Immediately after preparation, the surfaces of nanoporous gold samples prepared by electrochemical dealloying are covered by about one monolayer of surface oxide. In this state, the ligament size is very small, of the order of 1–2 nm. Furthermore, the charge response of the strain is here positive, samples contract during anodic scans. This behavior is highly reproducible; it persists in $HClO_4$ as long as the potential remains within the OH-adsorption region. When the in situ dilatometry experiments are repeated after an intermediate cathodic cycling – which removes the oxide and coarsens the ligaments – the conventional charge strain response, with expansion during anodic cycling, is observed.

It is of interest to compare the apparent surface stress-charge coefficients, ς, for the two states of the surface, oxide-covered and clean. In similar studies on porous Pt prepared by consolidation of nano-powder [4], ς could be related to the measured quantities, the macroscopic strain $\delta l/l_0$, the transferred charge δQ, and the sample mass m via

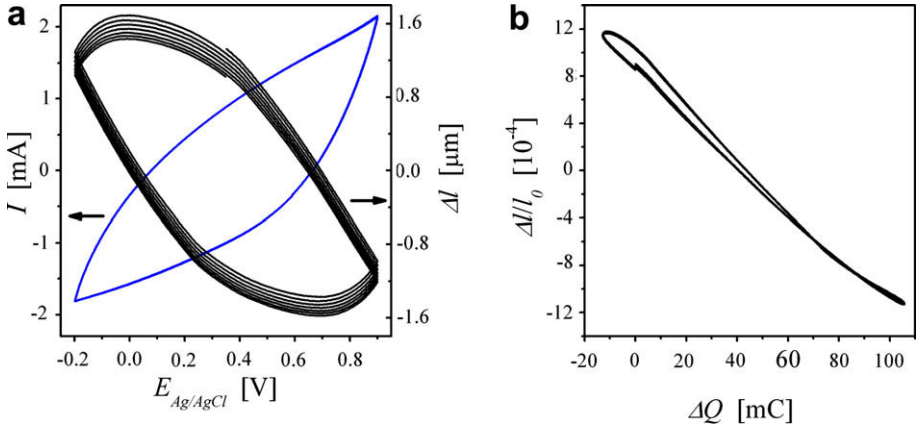

Fig. 6. Measurements in 0.3 M NaF before cathodic potential sweep. (a) Current I versus potential E (left ordinate) and length change Δl (right ordinate) during cyclic voltammogram at 10 mV/s in potential range −0.2 V to +0.9 V. (b) Corresponding values of strain, $\Delta l/l_0$, versus net charge ΔQ.

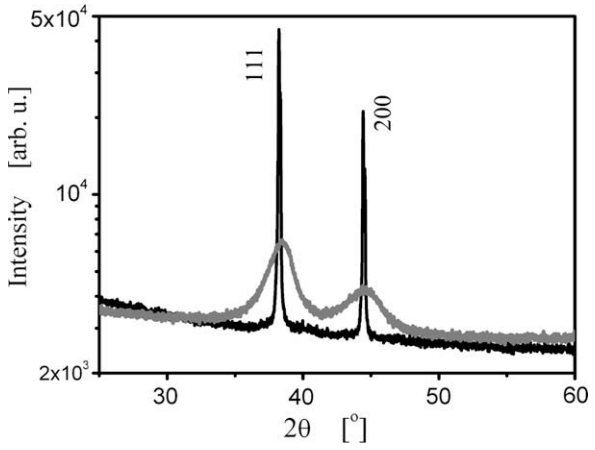

Fig. 7. X-ray diffractograms of $Ag_{75}Au_{25}$ alloy before (black) and after (gray) dealloying at 0.85 V (versus Ag/AgCl) in 1 M $HClO_4$. Note logarithmic intensity scale.

Table 1
Summary of the apparent values of surface stress-charge coefficient ς – as estimated based on Eq. (1) – in different surface states. Potential range and electrolytes are indicated.

Surface state	Electrolyte	Potential range [V]	ς [V]
Oxide-covered	1 M $HClO_4$	0.7 to 1.0	+2.0
	0.3 M NaF	−0.2 to 0.9	+4.7
Clean surface	1 M $HClO_4$	−0.3 to 0.4	−1.7
		0.7 to 1.0	−0.6
	0.3 M NaF	−0.6 to 0.2	−1.3

$$\varsigma = -\frac{9\,K\,m}{2\,\rho\,l_0}\,\frac{\delta l}{\delta Q}, \tag{1}$$

where K denotes the bulk modulus of the metal. For the present samples, this equation suggests a positive-valued ς before (oxidized surface) and a negative-valued one after cathodic cycling (clean surface). This is summarized in Table 1. Note that our computation of ς is here independent of structure size or surface area. It is emphasized, however, that these results afford here merely a comparison of the relative magnitudes, not reliable absolute values of ς. This will now be explained.

The derivation of Eq. (1) rests on the assumption that an isotropic affine stretch is a good approximation to the deformation by which the porous materials' metal skeleton reacts to changes in the surface stress. This is plausible for compacts of approximately spherical powder particles of similar size, where it has indeed been confirmed by in situ x-ray experiments [4]. By contrast, the surface-induced stress in elongated objects – such as the ligaments in npg – will typically exhibit a significant shear component [27], and the resulting strain may locally be quite anisotropic. First results of a continuum mechanics approach to the problem indicate that Eq. (1) may then overestimate the magnitude of ς by (in extreme cases) as much as one order of magnitude, depending on the geometry of the ligaments and on the value of the Poisson number. In the absence of a 'calibration' by in situ diffraction, the above results for ς are therefore qualitative. This does not, however, affect the validity of the signs of these coefficients, nor does it impede a comparison of their relative magnitudes, provided that the aspect ratios of the ligaments remain comparable.

Ab initio simulation finds closely compatible charge response in Au clusters of about 2 nm diameter and at single crystal Au surfaces [10,11]. We therefore rule out the extremely small structure size of the as-prepared samples as a possible origin of the inverted stress-charge behaviour. As a possible explanation, we suggest instead that the electronic screening in an oxide is less efficient than that in a metal surface. Thus, one may expect that the excess charge may penetrate deeper below the surface when an oxide layer is present. The positive-valued ς might then be understood in terms of a rigid-band model: Excess electrons populate bonding conduction band states or antibonding valence band states, depending on the location of the Fermi energy near the surface. If band bending resulted in a location of E_F near the valence band, then extra electrons would populate the antibonding valence band states, weakening the bonding between atoms and inducing a trend for expansion.

Attempts at recovering the oxidized state of the surface failed, as large Faraday currents intervene before sufficiently anodic potentials are reached. We believe that this finding is related to a high activity of the npg for water oxidation. This would be consistent with recent reports of high catalytic activity of the material for other reactions, such as CO and methanol oxidation [28,29]. In this context it is also of interest that the formation of a superficial oxide during dealloying is compatible with the voltammogram: as can be seen in Fig. 3, the dealloying potential, E_D = 850 mV, is well within the features representing OH-adsorption and subsequent formation of a more stable oxide or hydroxide by a 'turnover' process [17]. Furthermore, E_D is also on the anodic side of the oxygen species desorption peak in the cathodic scan. This is consistent with the value of E_D being within the interval of stability of a surface oxide. The oxide formation during dealloying may also benefit from a more stable state of adsorbed oxygen species on the atomically rough surface while the corrosion is active.

Finally we emphasize the smallness of the initial structure. This shows that the oxygen coverage efficiently prevents coarsening, quite likely due to a reduced surface diffusivity of the metal. Removing the oxide leads to practically instantaneous increase in the structure size. We believe that this reflects two concurring processes, the creation of a large transient population of mobile gold adatoms during the process of reduction itself [19,30], as well as – on a longer timescale – the creation of a clean gold surface which is free of the constraints on diffusivity due to the oxide. The observation suggests that the role of oxide coverage in influencing the corrosion kinetics may deserve more attention in future studies of dealloying.

5. Summary

In situ dilatometry was carried out for nanoporous gold samples with two distinct surface states, namely the oxide-covered surface of the freshly-dealloyed sample and the clean gold surface after reduction during cathodic potential sweeps. The oxide thickness on the freshly-dealloyed surface was estimated to be one equivalent monolayer according to the cumulative irreversible charge during cathodic potential sweeps. We find that as-prepared npg, with the oxide layer in place, exhibits an extremely small ligament size, below 2 nm. Lifting of the oxide induces quasi instantaneous structural coarsening, leading here to a structure size around 20 nm.

The freshly-dealloyed sample shows negative strain-to-potential and strain-to-charge slopes when cyclically scanned in a positive potential, indicating an unusual positive surface stress-charge coefficient ς of the oxide-covered surface. The reduced sample exhibits an opposite-signed value of ς, indicating the recovery of the conventional, negative ς values of clean Au surfaces. We have suggested that the different behavior may relate to the different electronic screening lengths in oxide and metal, respectively.

Our results highlight the role of the superficial oxide that is formed during dealloying in stabilizing an extremely small ligament size, well below 2 nm. Removing the oxide leads to quasi instantaneous coarsening, due to the higher mobility of Au on

the clean surface, and to the transient generation of a large number of mobile adatoms. At 0.24%, the charge-induced strain amplitude in the oxide-covered nanoporous gold sample is the largest reported so far for unsupported metals. This is a direct consequence the small ligament size and of the ensuing extremely large specific surface area.

Acknowledgements

This work was supported by Deutsche Forschungsgemeinschaft (CFN Karlsruhe). H.J.J. greatly acknowledges support by the Alexander-von-Humboldt Foundation.

References

[1] H. Ibach, Surf. Sci. Rep. 29 (1997) 193.
[2] R.C. Cammarata, K. Sieradzki, Annu. Rev. Mater. Sci. 24 (1994) 215.
[3] W. Haiss, Rep. Prog. Phys. 64 (2001) 591.
[4] J. Weissmüller, R.N. Viswanath, D. Kramer, P. Zimmer, R. Würschum, H. Gleiter, Science 300 (2003) 312.
[5] D. Kramer, R.N. Viswanath, J. Weissmüller, Nano Lett. 5 (2004) 793.
[6] S. Lu, B. Panchapakesan, Nanotechnology 17 (2006) 888.
[7] D. Kramer, J. Weissmüller, Surf. Sci. 601 (2007) 3042.
[8] W. Haiss, R.J. Nichols, J.K. Sass, K.P. Charle, J. Electroanal. Chem. 452 (1998) 199.
[9] H. Ibach, Electrochim. Acta 45 (1999) 575.
[10] F. Weigend, F. Evers, J. Weissmüller, Small 2 (2006) 1497.
[11] Y. Umeno, C. Elsässer, B. Meyer, P. Gumbsch, M. Nothacker, J. Weissmüller, F. Evers, Europhys. Lett. 78 (2007) 13001.
[12] M. Hahn, O. Barbieri, R. Gallay, R. Kötz, Carbon 44 (2006) 2523.
[13] D. Golub, A. Soffer, Y. Oren, J. Electroanal. Chem. 260 (1989) 383.
[14] R.H. Baughman, C. Cui, A.A. Zakhidov, Z. Iqbal, J.N. Barisci, G.M. Spinks, G.G. Wallace, A. Mazzoldi, D. De Rossi, A.G. Rinzler, O. Jaschinski, S. Roth, M. Kertesz, Science 284 (1999) 1340.
[15] R.C. Newman, S.G. Corcoran, J. Erlebacher, M.J. Aziz, K. Sieradzki, MRS Bulletin 24 (1999) 24.
[16] R.N. Viswanath, D. Kramer, J. Weissmüller, Electrochim. Acta 53 (2008) 2757.
[17] D. Kramer, R.N. Viswanath, S. Parida, J. Weissmüller, Mater. Res. Soc. Symp. Proc. 876E, R.2.5.1, 2005.
[18] S. Parida, D. Kramer, C.A. Volkert, H. Rösner, J. Erlebacher, J. Weissmüller, Phys. Rev. Lett. 97 (2006) 035504.
[19] B.E. Conway, Prog. Surf. Sci. 49 (1995) 341.
[20] P. Durkin, A.J. Forty, Philos. Mag. A 45 (1982) 95.
[21] M.A. Schneeweiss, D.M. Kolb, Solid State Ionics 94 (1997) 171.
[22] S. Trasatti, A. Petrii, Pure Appl. Chem. 63 (1991) 711.
[23] P.S. Germain, W.G. Pell, B.E. Conway, Electrochim. Acta 49 (2004) 1775.
[24] S. Cattarin, D. Kramer, A. Lui, M.M. Musiani, J. Phys. Chem. C 111 (2007) 12643.
[25] R.N. Viswanath, D. Kramer, J. Weissmüller, Langmuir 21 (2005) 4604.
[26] L. Maya, M. Paranthaman, T. Thundat, M.L. Bauer, J. Vac. Sci. Technol. B 14 (1996) 15.
[27] J. Weissmüller, J.W. Cahn, Acta Mater. 45 (1997) 1899.
[28] V. Zielasek, B. Jürgens, C. Schulz, J. Biener, M.M. Biener, A.V. Hamza, M. Bäumer, Angew. Chem. Int. Ed. 45 (2006) 8241.
[29] J. Zhang, P. Liu, H. Ma, Y. Ding, J. Phys. Chem. C 111 (2007) 10383.
[30] B.K. Min, A.R. Alemozafar, M.M. Biener, J. Biener, Topics Catal. 36 (2005) 77.